

Stability of THAI in situ combustion process in reservoirs with layers of grading permeabilities and porosities: Detailed qualitative investigations

Muhammad Rabiū Ado^a, Malcolm Greaves^b, Sean P. Rigby^{a,*}

^a Department of Chemical and Environmental Engineering, University of Nottingham, University Park, Nottingham, NG7 2RD, UK

^b Department of Chemical Engineering, University of Bath, Claverton Down, Bath, BA2 7AY, UK

ARTICLE INFO

Keywords:

In situ combustion (ISC)
Enhanced oil recovery (EOR)
Heavy oil/bitumen/tar sand
Reservoir simulation
Toe-to-heel air injection (THAI)
Permeabilities and porosities gradations

ABSTRACT

The world-wide reserves of heavy oil, tar sand, and bitumen, etc., outweigh those of conventional oil by a factor of 7/3. Given that the conventional reserves are being rapidly depleted, the need to develop and produce the unconventional resources has never been so critical. However, the proven most efficient and environmentally-friendly technology, namely the THAI process, still requires further study, and it has no documented design procedures that factor in the non-ideal geological features of heavy oil and bitumen reservoirs. Throughout the literature, there is little reported on the effects of gradations in reservoir petro-physical parameters on the performance of the THAI process. Consequently, this work reports the results of numerical simulations for four different kinds of reservoirs, each having progressive gradations in permeabilities and porosities. The major findings from this in depth study include.

(i) In terms of the temperature distribution, regardless of the permeability and porosity gradations, the high temperature zone is always skewed towards the highest permeabilities and porosities zone. Furthermore, it is found that, in any model in which the shoes of the VI wells have no direct communication pathway with the highest permeabilities and porosities zones of the reservoirs, the high temperature zones occur in two chambers, otherwise, there is one high temperature zone.

(ii) It is found that generally, the combustion front tends to be lopsided in favour of the most permeable and porous zone. In the case of a bottom-up progressive increase in permeabilities and porosities (model L1), the single combustion front has greatest advance horizontally at the top and axially in the middle of the reservoir, while in model L2 (the converse of model L1), the combustion fronts propagated in two chambers before the chambers overlapped in the toe region of the HP well where it advanced fastest. Therefore, the combustion zone in model L1 was far more stable than in model L2.

(iii) It is found that the combustion fronts in model L3, with the lowest permeabilities and porosities at the centre in the longitudinal direction, propagated in two chambers that overlapped each other around the toe region of the HP well and advanced greatest in the HP well and on either lateral edge of the reservoir. In model L4, which has lateral gradation in permeabilities and porosities, however, the thinner edge of the wedge-shape combustion front had advanced fastest along the vertical mid-plane where the HP well was located. Thus, the combustion zone in model L3 was far more stable than that in model L4.

(iv) It is found that in all the models except model L4, there exist rich oil saturation zones in the most permeable and porous regions located ahead of the mobile oil zone (MOZ) of each reservoir. These are formed due to restrictions in the pathways via which the mobilised oil can drain into the HP well. In model L4, the HP well is already in the most permeable zone and consequently, the fluids that favourably reach there are rapidly gravity-drained into the HP well.

1. Introduction

The world-wide cumulative reserves of unconventional oils like

heavy oil, tar sand, bitumen, etc., outweigh those of the conventional oils by a factor of 7/3 (Elahi et al., 2019; Guo et al., 2016; Liu et al., 2019). Given that the reserves of the conventional oils are being rapidly

* Corresponding author.

E-mail addresses: eng_muhammad@live.co.uk (M.R. Ado), sean.rigby@nottingham.ac.uk (S.P. Rigby).

<https://doi.org/10.1016/j.geoen.2024.213158>

Received 22 March 2024; Received in revised form 6 June 2024; Accepted 22 July 2024

Available online 23 July 2024

2949-8910/© 2024 The Authors. Published by Elsevier B.V. This is an open access article under the CC BY license (<http://creativecommons.org/licenses/by/4.0/>).

depleted, the need to develop and produce unconventional resources has never been so critical especially for a smoother transition to the carbon-neutral energy and economic systems of the future. However, the heavy oil and tar sand are characterised as having very high viscosity and very low API gravity, and hence their development and production are both capital- and energy-intensive. Since the viscosities of heavy oil and tar sand drop exponentially with increase in temperature, thermal production techniques are the methods of choice. These can be steam-based, in which steam is injected into the reservoir formation, or those which have the heat generated inside the reservoir. However, up to the present, the most widely used techniques for producing these resources are the steam-based processes, which are the steam-assisted gravity drainage (SAGD), cyclic steam stimulation (CSS), and the steam flooding (SF). Among them, SAGD is the much more popular, as it mostly performs better than the other steam-based processes (Gates and Larter, 2014). However, all the steam-based processes have undesirable features which include (i) being water-intensive, (ii) generating and releasing large quantities of carbon-oxides when generating the steam, (iii) experiencing considerable heat loss in the wellbore, (iv) generating and hence handling a large quantity of wastewater, (v) not providing pronounced heavy-to-light oil upgrading thereby leading to the need of surface upgraders, (vi) not being applicable to reservoirs whose thicknesses are lower than 15 m, etc. (Gates, 2010; Gates and Larter, 2014; Oskouei et al., 2011; Shah et al., 2010; Shi et al., 2017; Turta and Singhal, 2004; Wang et al., 2019; Zhao et al., 2013, 2014). On the other hand, those processes in which the heat is generated in situ, like the in situ combustion technologies, tend not to have the disadvantages of the steam-based processes.

The two main in situ combustion technologies are the conventional in situ combustion (ISC) process and the toe-to-heel air injection (THAI) process. However, the ISC has the undesirable features of (i) excessive gas override, (ii) excessive pressure build-up especially when the flue gases leaving the combustion front do not have a direct pathway via which they can reach the vertical producer well, (iii) high chance of forming an uneven, poorly structured combustion front, and (iv) mobilised upgraded oil taking a long path before it reaches the vertical producer well due to the “long-distance-displacement” nature of the process (Greaves et al., 2008; Turta and Singhal, 2004; Xia et al., 2005). On the other hand, the THAI process has none of the disadvantages of the ISC except that it is sometimes found to have a very low oil production rate despite it being far more energy-efficient than SAGD (Wei et al., 2020a, 2020b). The reasons for this performance need to be explored. The combustion in the THAI process is sustained by continuously injecting air via vertical injector (VI) well(s) and the fluids (which are the mobilised upgraded oil, water, and gases) are produced through a horizontal producer (HP) well. The THAI process has been quite extensively studied experimentally (Greaves et al., 1999; Xia et al., 2002; Xia and Greaves, 2002, 2006; Zhao et al., 2018a, 2018b, 2021) and via lab-scale numerical simulations (Ado, 2020a, 2021a; Ado et al., 2019; Greaves et al., 2012a, 2012c; Rabi Ado, 2017a; Rabi Ado et al., 2017b, 2018) and field-scale numerical simulations (Ado, 2020b, 2020c, 2020d, 2020e, 2021b, 2021c, 2021d, 2022a, 2022b; Ado et al., 2022; Anbari et al., 2023; Greaves et al., 2012b). However, only a handful of these studies touched on the effects of reservoir pay thickness on the performance of the THAI process, or on the influence of non-ideal geological features, which frequently characterise heavy oils and bitumen reservoirs. For example, Xia et al. (2002) reported an experimental investigation of the effect of reservoir pay thickness on the performance of the THAI process. Further, Ado (2020d) and Anbari et al. (2023) reported the effect of reservoir bottom water on the applicability and performance of the THAI process in reservoirs underlain by bottom water, and Ado et al. (2019) reported on the effects of reservoir heterogeneity and gas cap on the performance of the THAI process. This last-listed study (i.e. Ado et al., 2019), however, only superficially touched upon the effects of gradations in reservoir petro-physical parameters (i.e. the absolute permeabilities and porosities) on the stability

of the combustion zone and performance of the THAI process in general. It did not extensively investigate the key qualitative parameters, namely distribution of oil saturation, temperature distribution, and oxygen distribution and shape of combustion front, that are used to assess the performance of the THAI process. Furthermore, it did not compare, in depth, the performance of the THAI process in reservoirs with, respectively, bottom-up progressive increase, and bottom-up progressive decrease, in permeabilities and porosities. Similarly, no detailed comparisons of the performance of the THAI process in reservoirs having highest permeabilities and porosities at the centre in the longitudinal direction, and those having lowest permeabilities and porosities at the centre in the longitudinal direction, have been made. Consequently, since there is no single study in the literature that fully detailed the influence of petro-physical parameters gradations on the performance of the THAI process, and in line with the need to improve understanding of, and providing a design procedure for, the THAI process, through the use of reservoir numerical simulations, this study investigated, in great detail, the stability of the THAI in situ combustion process in reservoirs with layers of grading permeabilities and porosities.

2. Methodology

Many input parameters are required when numerically simulating the THAI process. This is because it involves consideration of multi-phase, multicomponent reactive transport processes inside a porous medium. However, prior to specifying them, the system, its dimensions, well arrangement, and its boundary conditions must be identified.

2.1. Reservoir representative volume, its well pattern, and their dimensions

The dimensions and size of the selected representative model reservoir volume are the same as those of the validated numerical model reported in the previous work of Rabi Ado et al. (2017b), and it is that validated laboratory-scale numerical model of the THAI process that is used in this work. Additionally, the reservoir representative volume is of the same dimensions and size as the 3-dimensional combustion cell used by Xia and Greaves (2002) to conduct experiments which are about upgrading and producing Athabasca bitumen using the THAI process. To build the reservoir representative volume which is shown in Fig. 1, the Computer Modelling Group's (CMG's) Builder, in combination with the CMG's STARS, the reservoir numerical simulator, were used. Given the previous lack of consideration in the existing literature (Ado et al., 2019; Rabi Ado, 2017a), four particular, numerical models have been built.

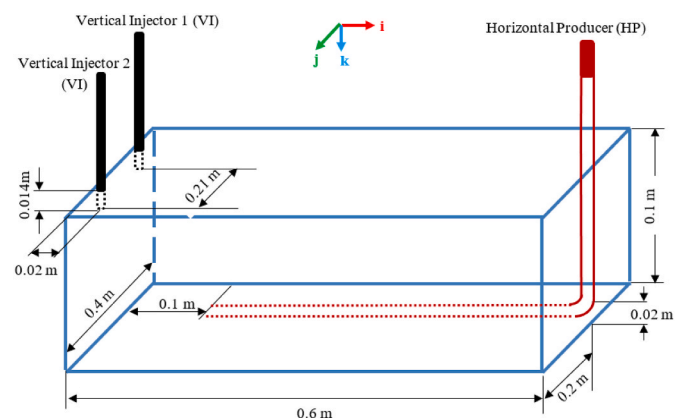


Fig. 1. Three-dimensional combustion cell (or reservoir representative volume) dimensions and the configuration of its wells. The i direction is along the axial length of the horizontal producer (HP) well (i.e. the i direction is in the longitudinal direction of the reservoir), the j direction is perpendicularly lateral to the axial length of the HP well, and the k direction is vertically downward.

In each of the four models, two vertical injector (VI) wells, arranged in a staggered line drive pattern with a single horizontal producer (HP) well, are used. The VI wells in the four models have the same length and internal diameter, and are drilled in correspondingly the same location in the reservoirs. Likewise, the HP well in each model has the same size as those of, and is drilled in similar location as in, all the other models. In other words, all the four models are constructed using Fig. 1 with everything depicted therein kept the same throughout each model. However, before specifying the layers of grading permeabilities and porosities and prior to running the simulation, the reservoir must be divided into small chunks called the grid blocks.

2.2. Reservoir representative volume division and equation discretisation

The transport processes governing the behaviour of the THAI process are mathematically described by a set of highly non-linear partial differential equations (PDEs). As a result, these PDEs must be discretised and thus be converted to a set of algebraic equations that are readily solvable. However, efficient and accurate solution of the resulting equations can only be achieved if they are applied to the whole small portions of the reservoir representative volume. Therefore, the whole reservoir representative volume must be divided into small-size blocks or portions. This is achieved by dividing the reservoir representative volume into a number of mesh points in the three respective directions so that the grid blocks are formed. Therefore in this study, and in accordance with the optimum number of grid blocks determined in previous work (Rabiu Ado et al., 2017b), the reservoir representative volume is divided into 30 grid points in the direction i , by 19 grid points in the direction j , and by 7 grid points in the direction k . Furthermore, to capture the full dynamics of the combustion front, each separation between two successive connected grid points along the i direction is refined into 3 child grid points, and the same is applied to each separation between two successive connected grid points along the j direction. This resulted in forming 90 by 57 by 7 child grid blocks. In addition, the CMG STARS software has a built-in discretised wellbore

model (DWM) function known as “WELLBORE” which, if called within the simulation, means the HP well is internally divided into a number of grid blocks so that the transient nature of the physicochemical transport processes inside the well are fully accounted for. Hence, inclusive of the DWM, the total number of grid blocks in building the model is 38,500. The combined resulting algebraic equations from the reservoir discretised equations and the DWM equations are solved simultaneously by STARS using a fully implicit finite difference method.

2.3. Reservoir initial conditions and its petro-physical parameters

Throughout each of the four models, the initial oil saturation is 85%, the initial water saturation is 15%, and the initial gas saturation is 0%. All the four models have initial coke concentration of 0 kg/m^3 . In all the four models, the initial temperature is 27°C and the initial pressure is 290 kPa. In all the four models, the effects of gradations in permeabilities and porosities are studied. The first model, referred to as L1, has a bottom-up progressive increase in permeabilities and porosities (Fig. 2a), while the second model, L2, has a bottom-up progressive decrease in permeabilities and porosities (Fig. 2b). The third model, L3, has the lowest permeabilities and porosities at the centre in the longitudinal direction (Fig. 2c), while model L4, which has lateral gradation in permeabilities and porosities, has the highest permeabilities and porosities at the centre in the longitudinal direction (Fig. 2d). Models L3 and L4 are based on the types of convoluted bedding features often found in soft-sediment deformation structures (Boggs, 2006; Fietz et al., 2024) and the heterogeneous deposits found in inclined heterolithic stratification (Thomas et al., 1987; Hassanpour, 2009). These models represent an upper bound on what deformation of highly inclined features might obtain.

At every point in each model the ratio of absolute vertical permeability over absolute horizontal permeability, K_v/K_h , is maintained as 3/10. To determine the corresponding porosities for each pair of K_v and K_h permeabilities, the following equation, which relates the permeabilities to porosities, is used:

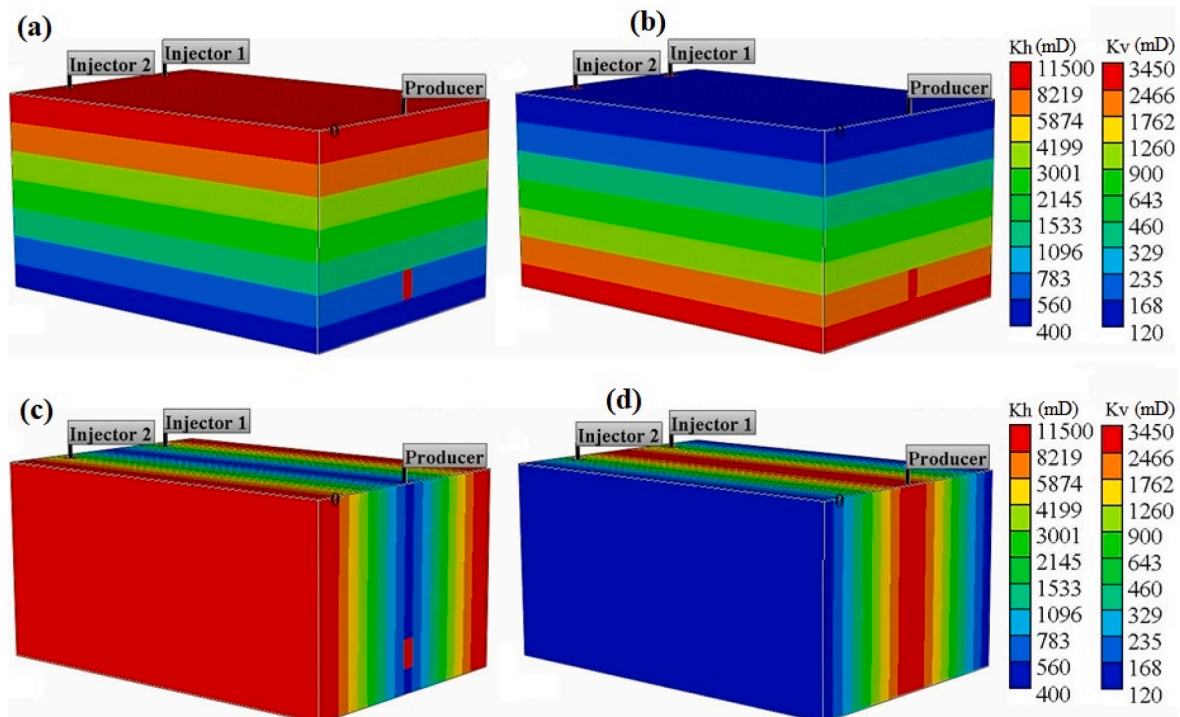


Fig. 2. Models (a) L1, (b) L2, (c) L3, and (d) L4 showing the distributions of the permeabilities in the layered reservoirs. Note that K_h is the horizontal absolute permeability whilst K_v is the vertical absolute permeability.

$$K = K_o e^{\left[f \left(\frac{\phi - \phi_o}{1 - \phi_o} \right) \right]}, \quad (1)$$

wherein K is the current permeability, ϕ is the current porosity, K_o is the initial permeability, ϕ_o is the initial porosity, and f is a multiplication factor. Using a shale absolute horizontal permeability of 1 mD and porosity of 0.01 as the initial values (Le Ravalec et al., 2009), and combined with those of the validated numerical model (Rabiu Ado et al., 2017b), the f value is determined to be 18.71 and it is used in each model. The highest and lowest vertical absolute permeabilities are 3450 mD and 120 mD, respectively, which have corresponding porosities of 34% and 22.15%, respectively. For models L1 and L2, the change in the permeabilities between every two overlying layers is by a factor of 1.75, whilst in models L3 and L4, the change in the permeabilities between every two adjacent vertical planes which are in the longitudinal direction is by a factor of 1.5. The gas/oil and oil/water relative permeability curves of the Athabasca bitumen are the same as those used in the previous study by Rabiu Ado et al. (2017b).

2.4. Boundary conditions

Flows in and out of the reservoir representative volume of each model take place via the VI wells and the HP well respectively, and, other than those locations, a no flow boundary condition is assigned all over each reservoir representative volume. In each of the models, the region around the injector well is steam-preheated using a saturated steam at a pressure of 2600 kPa and at injection rate of 21.17 cm³ min⁻¹ cold water equivalent (CWE) for a period of 30 min before air injection is commenced and ignition is achieved. This is to achieve fluid communication with the horizontal producer (HP) well and to condition the outlet zone of the injector well for combustion initiation. The combustion is sustained by continuous air injection initially at the rate of 8000 Scm³ min⁻¹ before it is increased to 12,000 Scm³ min⁻¹ for a combustion period of 6 h (i.e. total operating time of 390 min). The HP well has a producer back pressure of 200 kPa. The heat loss takes place via conduction at the overburden and the underburden rocks. All these parameters are similarly specified in each of the four models.

2.5. Other input parameters

Heavy oil and bitumen are, respectively, a mixture of extremely large number of individual hydrocarbons to the extent that it is impossible to represent either of them using their individual compounds. Rather, the mixture must be divided into a smaller number of oil pseudo-components, which are made up of a group of compounds that boils over a certain temperature range. Since this study made use of the properties of the typical Canadian Athabasca bitumen, as in a previous study (Rabiu Ado et al., 2017b), the bitumen or oil pseudo-components, their boiling temperature, their pressure, density, and temperature (PpT) properties, which are taken from Rabiu Ado et al. (2017b), are reproduced in Table 1. Table 2 shows the viscosities of the oil or bitumen pseudo-components as function of temperature as used in this work. The thermal properties of the oil pseudo-components in the form of the specific heat capacity and thermal conductivity, which are obtained from Aspen Hysys based on the built-in fluid-package named Peng-Robinson equation of state, are shown in Table 3. These are taken from model P in Ado (2020a). The formula to calculate both the specific

Table 1

Oil pseudo-components and their composition, molecular weight, boiling temperature, and pressure, density, and temperature (PpT) properties.

Oil pseudo-component	Composition (mol %)	Molecular weight (g/mol)	Boiling temperature T _B (°C)	Critical pressure P _c (kPa)	Density ρ (kg/m ³)	Critical temperature T _c (°C)	Eccentricity
LC	42.50	210.82	281.47	1682.88	828.24	464.68	0.62
MC	23.91	496.81	549.67	1038.46	961.66	698.53	1.18
IC	33.59	1017.01	785.78	729.22	1088.04	940.36	1.44

Table 2

Viscosities of the oil pseudo-components as function of temperature.

T(°C)	IC (cP)	MC (cP)	LC (cP)
20	9.4675E+06	4.5502E+06	1.2900E+03
41	4.4391E+05	1.0309E+05	4.1016E+02
50	1.2547E+05	2.5996E+04	2.5500E+02
60	3.4819E+04	5.6394E+03	1.5600E+02
70	1.1965E+04	1.5469E+03	1.0628E+02
90	2.6772E+03	2.9996E+02	4.5911E+01
110	5.9274E+02	6.6423E+01	2.5380E+01
140	9.7768E+01	1.6566E+01	1.1066E+01
180	2.4103E+01	5.9724E+00	4.0619E+00
220	7.4356E+00	2.5830E+00	1.9600E+00
265	3.1460E+00	1.4189E+00	1.0599E+00
340	1.3872E+00	7.4235E-01	5.1269E-01
385	1.1340E+00	5.2696E-01	3.8119E-01
430	9.7208E-01	3.9124E-01	2.7235E-01
475	8.9119E-01	3.0579E-01	2.0947E-01
535	7.2030E-01	2.3522E-01	1.4350E-01
600	6.6277E-01	1.8495E-01	1.0611E-01
900	5.4121E-01	1.0888E-01	8.1781E-02
946.85	3.0265E-01	9.7290E-02	5.8708E-02

Table 3

Coefficients for specific heat capacity and thermal conductivity for the oil pseudo-components as taken from Ado (2020a).

Coefficients	A	B	C	D	E
Specific heat capacity coefficients for the liquid oil pseudo-components					
LC	65.23	1.370	-6.404 × 10 ⁻⁴	2.959 × 10 ⁻¹⁴	-1.738 × 10 ⁻¹⁷
MC	32.45	3.364	-1.571 × 10 ⁻³	-3.072 × 10 ⁻¹⁴	1.264 × 10 ⁻¹⁷
IC	-98.16	6.910	-3.226 × 10 ⁻³	-1.558 × 10 ⁻¹⁴	5.003 × 10 ⁻¹⁸
Thermal conductivity coefficients for the liquid oil pseudo-components					
LC	2.311 × 10 ⁻¹	-3.484 × 10 ⁻⁴	2.959 × 10 ⁻⁷	-6.768 × 10 ⁻¹¹	-2.149 × 10 ⁻¹³
MC	2.140 × 10 ⁻¹	-1.384 × 10 ⁻⁴	-1.767 × 10 ⁻⁷	3.891 × 10 ⁻¹⁰	-2.577 × 10 ⁻¹³
IC	1.869 × 10 ⁻¹	-5.378 × 10 ⁻⁵	-2.042 × 10 ⁻⁷	2.760 × 10 ⁻¹⁰	-1.286 × 10 ⁻¹³

heat capacity, C , (kJ/kmol·K) and the thermal conductivity, α , (W/m·K) is α or $C = A + BT + CT^2 + DT^3 + ET^4$ such that the temperature T is in K. The vapour-liquid equilibrium K-values which are reproduced in Table 4 are given as a function of both temperature and pressure, and are calculated using the Wilson's equation (Almeida et al., 2003) and the PpT properties of the oil or bitumen pseudo-components. To account for the chemical changes taking place during operation of the THAI process, the reaction schemes and their Arrhenius kinetics parameters must be specified. These are taken from model P from the previous work of Ado (2020a), as can be seen given in Table 5. The type of reservoirs considered in this work are model experimental-scale reservoirs with Athabasca-type oil having a quality of 10⁰ API gravity and an initial viscosity of 1.4069 × 10⁵ cP at a temperature of 25 °C. The value of the viscosity is chosen to fall within the various ranges reported by different authors. For example, for the typical Athabasca bitumen, Oskouei et al., 2011 have reported that it has a value of 4.45 × 10⁴ cP at 25 °C, and Mojarab et al. (2011) have reported that its value is 3.00 × 10⁵ cP at

Table 4

Vapour-liquid equilibrium K-values for the oil pseudo-components as functions of both temperature and pressure as used in this work.

T(°C)▼	K-values at pressure of 100 kPa for the three oil pseudo-components			K-values at pressure of 2000 kPa for the three oil pseudo-components		
	IC	MC	LC	IC	MC	LC
10	1.463E-18	4.503E-12	1.443E-05	7.317E-20	2.251E-13	7.215E-07
80	9.987E-14	1.293E-08	1.290E-03	4.993E-15	6.467E-10	6.451E-05
150	1.715E-10	2.666E-06	2.609E-02	8.573E-12	1.333E-07	1.304E-03
220	3.553E-08	1.211E-04	2.247E-01	1.776E-09	6.053E-06	1.123E-02
290	1.955E-06	2.129E-03	1.133E+00	9.775E-08	1.065E-04	5.664E-02
360	4.434E-05	1.986E-02	3.994E+00	2.217E-06	9.931E-04	1.997E-01
430	5.402E-04	1.188E-01	1.096E+01	2.701E-05	5.940E-03	5.479E-01
500	4.185E-03	5.139E-01	2.504E+01	2.093E-04	2.570E-02	1.252E+00
570	2.308E-02	1.743E+00	4.989E+01	1.154E-03	8.716E-02	2.494E+00
640	9.797E-02	4.904E+00	8.942E+01	4.898E-03	2.452E-01	4.471E+00
710	3.385E-01	1.190E+01	1.475E+02	1.692E-02	5.952E-01	7.375E+00
780	9.917E-01	2.569E+01	2.276E+02	4.958E-02	1.284E+00	1.138E+01
850	2.541E+00	5.035E+01	3.328E+02	1.271E-01	2.518E+00	1.664E+01
920	5.831E+00	9.122E+01	4.654E+02	2.916E-01	4.561E+00	2.327E+01
990	1.220E+01	1.547E+02	6.271E+02	6.102E-01	7.736E+00	3.135E+01

Table 5

Direct conversion thermal cracking kinetics and combustion reactions schemes and their Arrhenius parameters as taken from Ado (2020a).

Thermal Cracking Reactions	Frequency Factor (min ⁻¹)	Activation Energy (kJ/mol)	Heat of Reaction (kJ/mol)
IC → 2.0471 MC	3.822 × 10 ²⁰	239.01	0.00
MC → 0.4885 IC	3.366 × 10 ¹⁸	215.82	0.00
MC → 2.3567 LC	1.132 × 10 ¹⁵	184.88	0.00
LC → 0.4243 MC	1.524 × 10 ¹⁵	180.45	0.00
IC → 77.4563 COKE	2.320 × 10 ¹⁵	180.88	0.00
Combustion Reactions			
IC + 98.869 O ₂ → 77.456 CO _x + 46.904 H ₂ O	1.812 × 10 ⁸ kPa ⁻¹	138.00	4.00 × 10 ⁴
MC + 49.069 O ₂ → 37.075 CO _x + 25.953 H ₂ O	1.812 × 10 ⁹ kPa ⁻¹	138.00	1.60 × 10 ⁴
LC + 32.025 O ₂ → 4.600 CO _x + 35.623 H ₂ O	1.812 × 10 ¹⁰ kPa ⁻¹	138.00	4.91 × 10 ²
COKE + 1.22 O ₂ → CO _x + 0.565 H ₂ O	1.000 × 10 ¹⁰ kPa ⁻¹	123.00	3.90 × 10 ²

25 °C. Furthermore, as regards to the geological features of the location of the Athabasca reservoir whose oil properties are used in this work, it is located in the Lower Cretaceous McMurray formation which is the oldest formation in the so-called Mannville group.

3. Results and discussions

The key qualitative parameters that give a measure of the performance and stability of the THAI process are (1) the temperature distribution, (2) the oxygen distribution and shape of the combustion zone, and (3) the distribution of oil saturation (i.e. the oil flow dynamics inside the reservoir). As a result, these have been presented, thoroughly analysed, and discussed in detail. This is because these parameters are used to judge the success or otherwise of the THAI process.

3.1. Temperature distributions

The temperature distribution does not only give the measure of the spread of the combustion front, and the combustion mode (i.e. high- or low-temperature-oxidation mode (HTO or LTO mode)), but also allows the extent of heat transfer inside the reservoir to be determined. Fig. 3 shows the three-dimensional (3-D) distribution of temperature in each model. In each of the four models, the combustion front is operating in the HTO mode as indicated by the maximum temperatures which, even

in model L4 (Fig. 3d) which has the lowest maximum temperature, range from 416 °C to 462 °C. Comparing models L1 (Fig. 3a) and L2 (Fig. 3b), which have top-down gradations in permeabilities and porosities, it is found that heat is much more easily distributed to the lower section, and a larger volume, of the reservoir, and that the high temperature zone has a larger volume when there is a progressive increase in permeabilities and porosities from the top to the bottom of the reservoir which is the case in model L2. In model L1, where the permeabilities and porosities decrease progressively from the top to the bottom of the reservoir, the highest temperature zone is located in the upper portion and simultaneously mainly in the axial middle region of the reservoir. Furthermore, in model L2, the maximum temperature is higher than that in model L1. This can be credited to the fact that, in the former, the high temperature zone is mainly limited to the vicinities of the toe of the HP well and the shoes of the VI wells, while in the latter, the high temperature zone has greater spread horizontally in the axial direction. These, therefore, imply that heat loss, which takes place via the overburden and underburden only, is far higher to the overburden in model L1 than in model L2. This is evidently the case since the highest temperature regions, and hence highest temperature gradients, are directly at the top of the reservoir representative volume in L1. This is unlike in L2 where the heat must firstly travel vertically downward to the bottom of the reservoir where the temperature gradient between the underburden and the surroundings is low. Additionally, the higher permeability at the top of the reservoir in model L1 means that the injected air and thus the combustion gases preferentially flowed axially horizontally in a toe-to-heel manner and laterally, rather than vertically down as in model L2.

Comparing the temperature distributions in models L3 (Fig. 3c) and L4 (Fig. 3d), showed that the high temperature zones in the former occur in two separate chambers each originating from the shoe of each of the VI wells, while, in the latter, there is a single high temperature zone which is located in the middle region at the upper portion of the reservoir. Furthermore, these results revealed that there is faster and wider transportation of heat laterally in model L3 but axially in model L4. These differences are caused by the fact that, in model L3, the progressive increase in permeabilities and porosities going laterally to either side of the axial mid-region of the reservoir resulted in preferential fluid flow, and, hence, combustion front advance, to the most permeable sectors of the reservoir. In model L4, however, the axial mid-region of the reservoir has the highest permeabilities and porosities thereby causing the fluids and heat to easily be transported in and around the middle of the reservoir.

To dig deeper and find out the temperature of the fluids as they enter the HP well, the 2-dimensional temperature profile along the vertical mid-plane of the longitudinal direction for each model is given in Fig. 4. Generally, each of the four models has a backward-leaning temperature profile in such a way that heat is transported to a longer distance in the

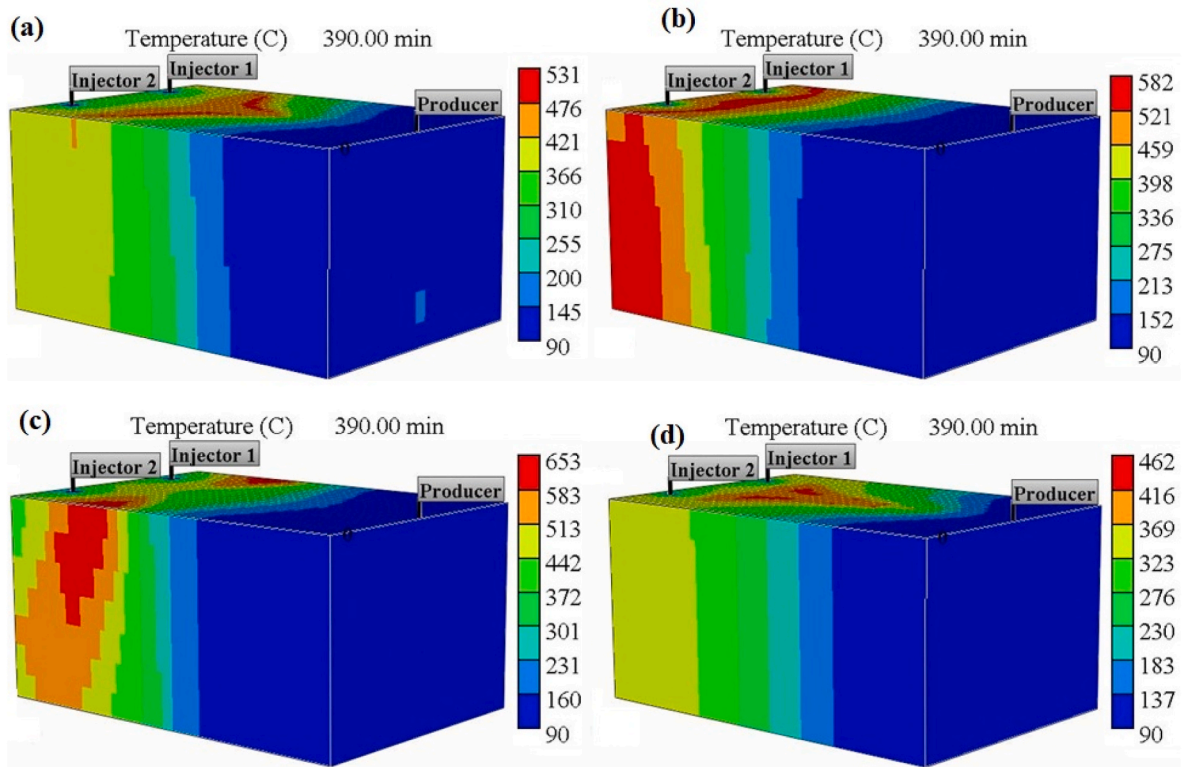


Fig. 3. Temperature distributions in the layered reservoirs at the end of 6 h of combustion for models (a) L1, (b) L2, (c) L3, and (d) L4. Note that the lowest temperature in the scales is set to be 90 °C, which is the minimum, and which is set in order for the temperature distributions in each model to be clearest (i.e. making the scales intervals to be shortest possible).

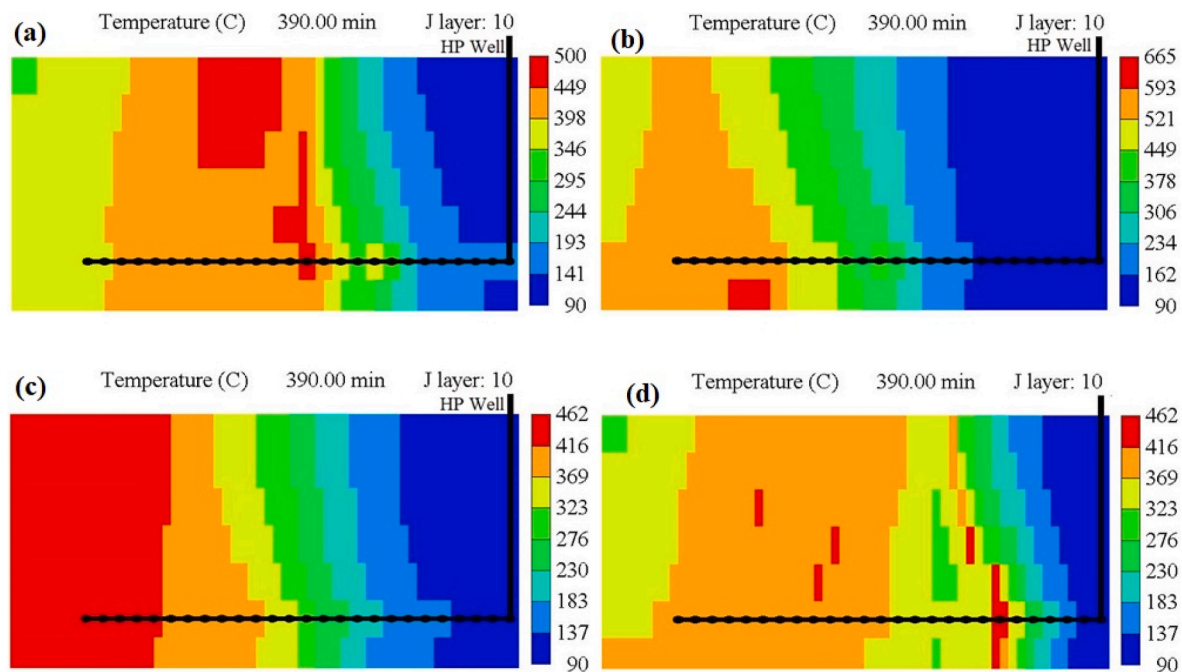


Fig. 4. Temperature distributions in the layered reservoirs at the end of 6 h of combustion and along the longitudinal vertical mid-planes of models (a) L1, (b) L2, (c) L3, and (d) L4 respectively. Note that the lowest temperature in the scales is set to be 90 °C which is the minimum and which is set in order for the temperature distributions in each model to be clearest (i.e. making the scales intervals to be shortest possible).

HP well when compared to that at the top of the reservoir. This is attributable to the fact that highest permeabilities, just like in the highest permeability-and-porosity zones, are assigned in the HP well of each model and therefore, as fluids are produced, they carry with them

some of the heat acquired just ahead of, and near, the combustion zones. Unlike in model L1 where the heat is mostly transferred due to both conduction and convection as the combustion front has traversed a long distance in a toe-to-heel manner (Fig. 4a), in model L2, most of the heat

transfer is due to convection and to a much lesser extent conduction, because the high temperature zone is located closer to the toe of the HP well (Fig. 4b). However, the temperature of the high temperature zone in model L2 is higher than that of model L1, and as a consequence, a larger amount of heat is distributed in the reservoir of L2, when compared to that of L1. In the case of models L3 (Fig. 4c) and L4 (Fig. 4d), they have the same temperature in their respective high temperature zone(s), but it covered a wider area in the former when compared to that in the latter. Furthermore, the high temperature zone of model L3 is in the toe region of the HP well which is unlike in model L4, where it is closer to the heel of the HP well. Likewise, the degree of heat transfer along the vertical mid-plane is far wider in model L4 compared to that in model L3. To summarize, in terms of the temperature distribution, regardless of the permeabilities and porosities gradations, the high temperature zone, or zones, is/are always skewed towards the highest permeabilities and porosities zone, or zones.

3.2. Oxygen distributions and shape of combustion zones

The oxygen distributions give the measure of the shape and the location of the combustion front. Fig. 5 shows the 3-dimensional shapes of the combustion fronts in all the four models. Comparing models L1 (Fig. 5a) and L2 (Fig. 5b), whose gradations in permeabilities and porosities are opposite to each other, reveals that, despite their differences in shapes and locations, the combustion fronts are lopsided in favour of the most permeable and porous zones. The combustion front has greater horizontal spread at the top, and vertical spread along the longitudinal middle of the reservoir of model L1. It is interesting to note that despite the fact that there is a progressive decrease in permeabilities and porosities from the top to the bottom of the reservoir, there is a near uniform advance rate of the combustion front in the longitudinal direction along the mid-axis of the reservoir of model L1 (Fig. 5a). This is caused by the fact that, along the vertical mid-plane in the longitudinal

direction, the residence time of oil is lower relative to that in the other parts of the reservoir, and that the mobilised partially upgraded oil there drains at nearly the same faster rates. This results in lower fuel availability in the axial vertical mid-plane (or mid-plane $i-k$) which caused the rates of coke deposition and consumption there to be around the same, and, hence, caused the combustion front to travel at nearly uniformly the same rates. In model L2, however, due to the downward progressive increase in permeabilities and porosities, two combustion chambers, each originating from the shoe of each VI well, were initially formed. The combustion front, which is semi-cylindrical in shape in each chamber, advanced rapidly downward to the most permeable and porous layers where they eventually merged and started to move forward at faster speed (Fig. 5b). This resulted in the forming of a wedge-like protrusion at the lower portion of the reservoir and along the axial length of the HP well. The longitudinal protrusion is lengthier inside the HP well. This is caused by the fact that the HP well has the highest permeabilities, just like in the highest permeability-and-porosity zones, which are assigned due to the fact that in the field, excessive sand is produced together with the fluids. Another difference between models L1 and L2 is that, in the former, the combustion did not reach the bottom-most horizontal layer, whilst in the latter it did to the extent that it has swept quite a large area non-relatively speaking.

While the combustion is propagating in two chambers, that overlapped each other around the toe region of the HP well, in model L3 (Fig. 5c), that in model L4 (Fig. 5d) has a wider spread around the shoes of the VI wells but is highly tapered in the longitudinal direction such that it formed a wedge shape. The two combustion chambers of model L3 have advanced more vertically downward and horizontally in the longitudinal direction on either lateral edge of the reservoir, which is due to the vertical longitudinal planes at the lateral edges having the highest permeabilities and porosities. Going laterally from either VI well to the mid-region of the reservoir revealed that the combustion chambers did not meet except in the toe region of the HP well and that they

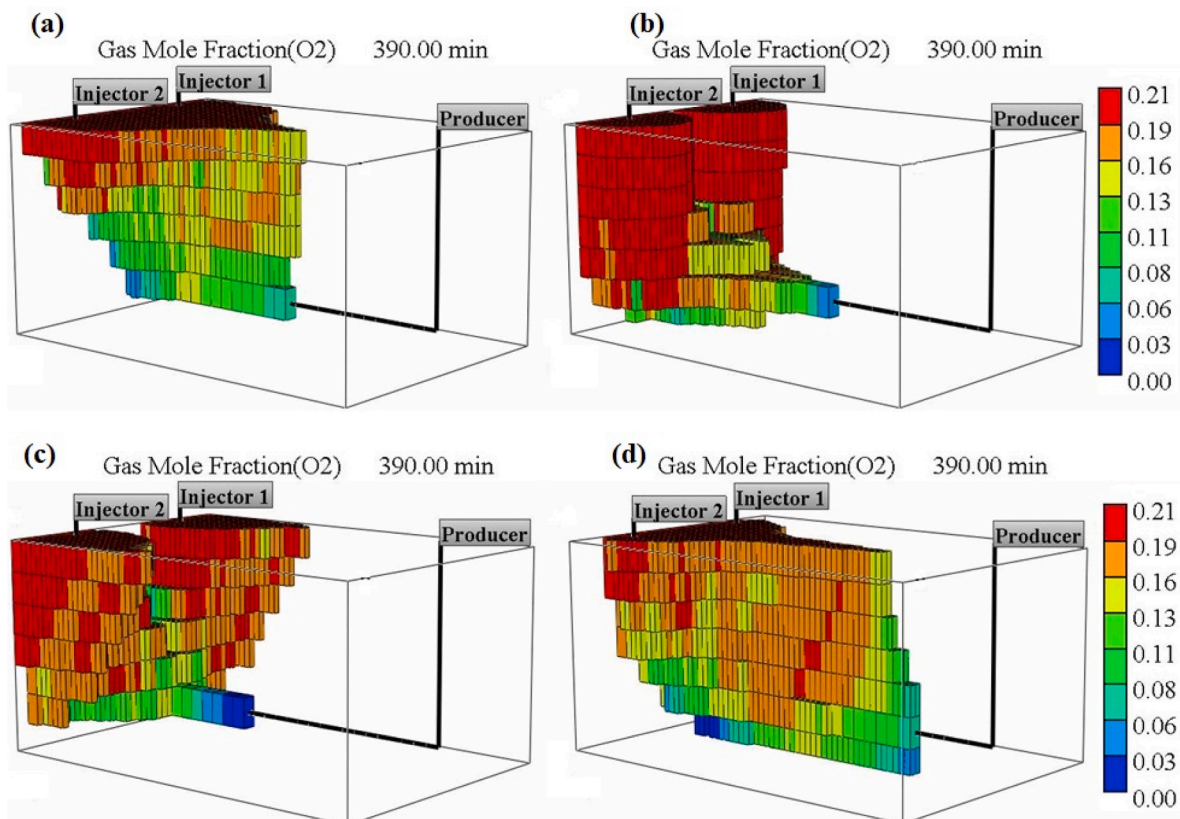


Fig. 5. Oxygen distributions in the layered reservoirs at the end of 6 h of combustion for models (a) L1, (b) L2, (c) L3, and (d) L4.

are conical in shape with wider tops and narrower bottoms (Fig. 5c). Then the combustion front protruded axially predominantly into the HP well, which is consistent with the HP well being highly permeable and porous, and everywhere else in the vertical mid-plane of the reservoir being relatively highly impermeable and non-porous. In model L4, however, the thinner edge of the wedge-shape combustion front has advanced fastest along the whole vertical mid-plane where it has a backward-slanting nature with the upper part lagging the lower part (Fig. 5d). Moreover, in contrast to model L3, the combustion front in model L4 has reached, and swept, a portion of the bottom-most layer along the vertical mid-plane of the reservoir.

To find out, in greater detail, about how stable the combustion front in each model is going to be in relation to the HP well, Fig. 6 shows slices of the vertical mid-planes of the four kinds of gradations in reservoir permeabilities and porosities. Higher areal sweep by the combustion front is achieved in model L1 (Fig. 6a), compared to in model L2 (Fig. 6b), where mainly the toe region of, and partly along, the HP well are swept by the combustion. These findings imply that, in real world settings where the HP well will be blanketed by large pool of mobilised partially upgraded oil, and/or where the thermal cracking zone resulted in large concentration of coke being deposited in the HP well just behind the mobile oil zone (MOZ) which is shown to also have presence in the toe, no oxygen production, due to combustion being propagated behind the thermal cracking zone and along the HP well, will take place. However, oxygen production, or even breakthrough, can take place due to gravity override resulting in air directly reaching the top of the heel of the HP well via the upper portion of the reservoir and/or due to channelling from the base of the reservoir up into the heel region of the HP well especially where the permeabilities and porosities are largest. The likelihood of the former is lower because of the buoyancy effect, and because the saturations of oil and water in the cold oil zone total to 100% and, therefore, the air must first displace oil, or water, or both, before it can have a pathway to reach the heel of the HP well. In contrast, the latter is highly likely once there is a direct pathway to the highly permeable and porous regions of the reservoir, like in model L2 where the significant quantity of the air being injected preferentially went vertically downward, and, on reaching the base of the reservoir, it then

bent at right angle and went horizontally forward in the longitudinal direction. Furthermore, how fast the combustion sweeps the HP well will also determine the long term stability of the whole process. The higher the rate of its advance in the HP well, the earlier the oxygen breakthrough takes place. Therefore, the values of the mole fraction of oxygen along the HP wells of both models L1 and L2 are compared, where it is found that the maximum mole fraction in the HP well in model L1 (Fig. 6a) is 0.16, whilst that in model L2 (Fig. 6b) is 0.18, thereby implying that more of the coke will be consumed faster, and therefore the combustion front will be speedier, in the latter compared to in the former. These are evidently true especially when Fig. 4a and b are compared, where model L1 has a lower maximum temperature than model L2. In model L3 (Fig. 6c), which has the lowest permeabilities and porosities in the vertical mid-plane, only a minor area around the toe of the HP well is being touched and is being swept by the combustion front. This is in direct contrast to model L4 (Fig. 6d), where the highest permeabilities and porosities are along the vertical mid-plane, and where the combustion front has swept the largest area. In fact, the combustion is taking place even in the base of the reservoir where it is leading in forward advancement compared to the top of the reservoir. Therefore, in terms of long term stability, the combustion front will reach the heel of the HP well far earlier in model L4, compared to in model L3. All in all, the combustion zone in model L1 is more stable than in model L2, and that in model L3 is more stable than that in model L4.

3.3. Oil saturation profiles

The distribution of oil saturation is useful in understanding the oil drainage dynamics inside the reservoir which will lead to optimum well placement with the aim of maximising oil recovery rates. Fig. 7 shows the 3-dimensional distribution of oil saturation in each model. In model L1 (Fig. 7a), it is found that the oil, like the other fluids, is both permeability- and porosity-philic and thence has concentrated in the high-permeability layers in the upper portion of the reservoir in two separate chambers, one on either lateral side and back face in the longitudinal direction. Despite the fact that the temperature at every location in the reservoir is at least 90 °C, the mobilised oil did not fully

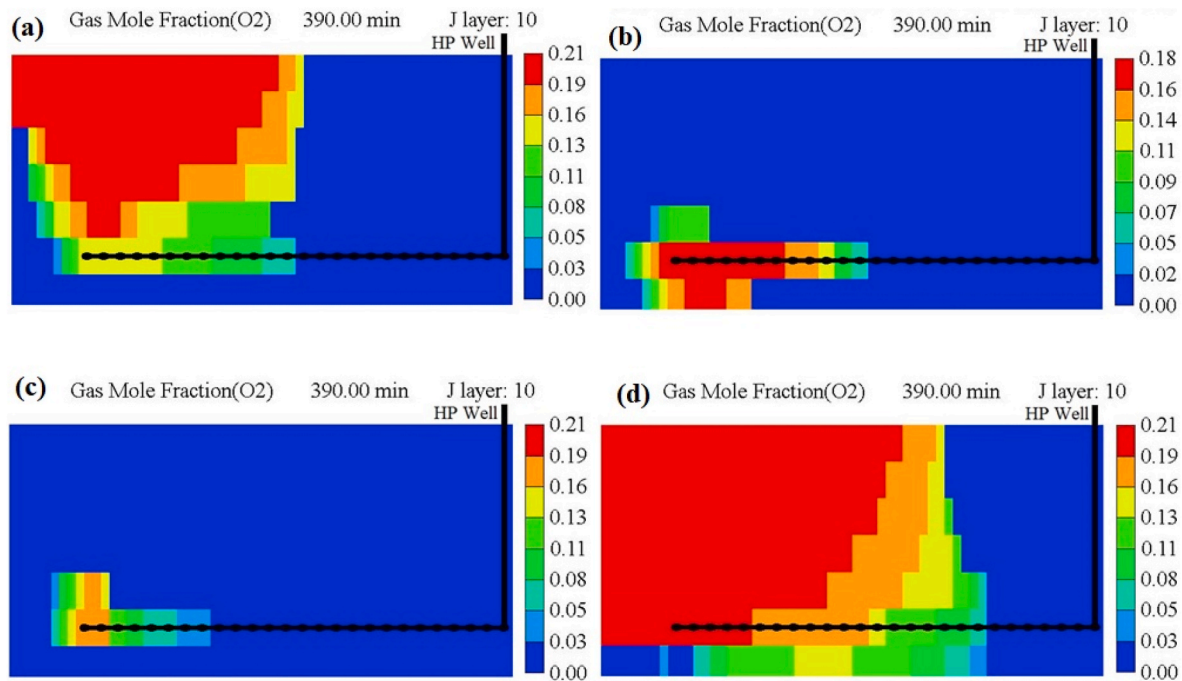


Fig. 6. Oxygen distributions in the layered reservoirs at the end of 6 h of combustion and along the longitudinal vertical mid-planes of models (a) L1, (b) L2, (c) L3, and (d) L4 respectively.

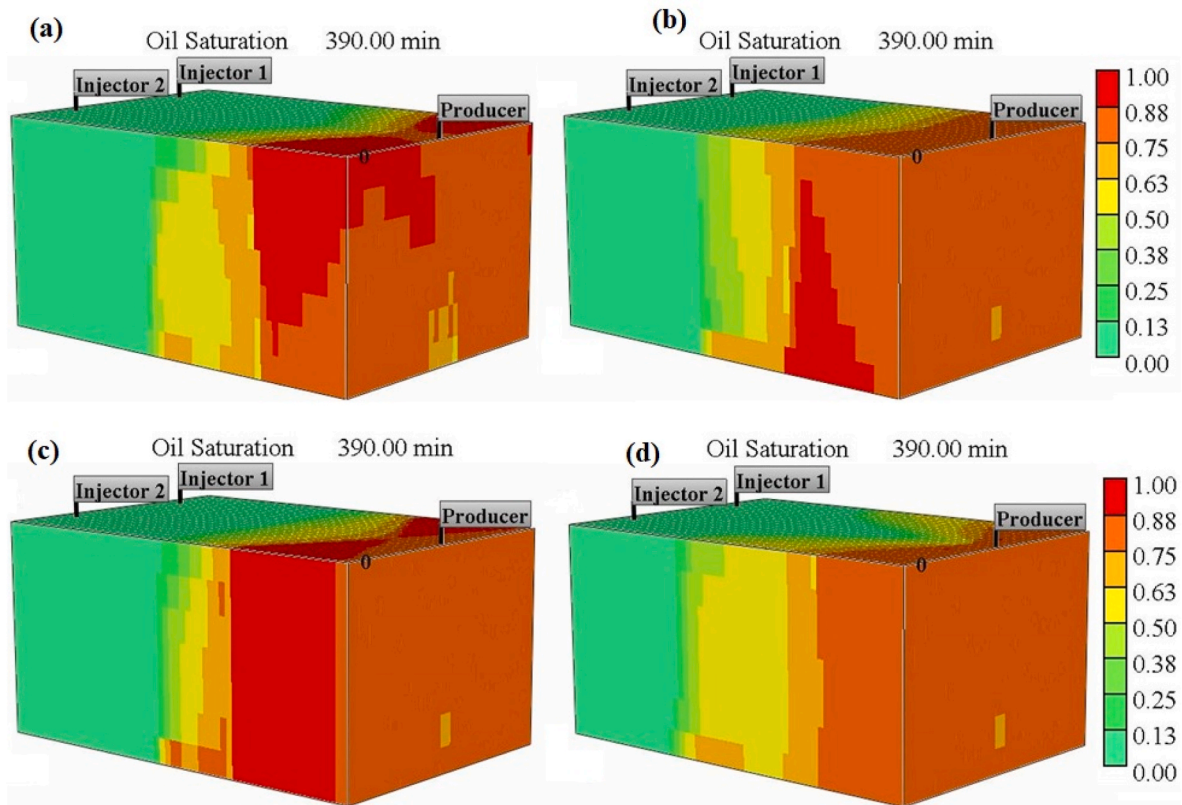


Fig. 7. Oil saturation distributions in the layered reservoirs at the end of 6 h of combustion for models (a) L1, (b) L2, (c) L3, and (d) L4.

drain under the influence of gravity, but, rather, it found it easier to advance horizontally in the longitudinal direction. Interestingly, the two chambers did not touch each other as they are separated by the vertical mid-plane which has the biggest drawdown of oil, as the oil flux vectors there have no horizontal component. Furthermore, a larger volumetric sweep is achieved at the top horizontal plane. Moving vertically downward, the volumetric sweep progressively decreased from one layer to another. In contrast, the high oil saturation zones are located in the bottom part on either lateral edge of the reservoir of model L2 (Fig. 7b). The behaviour in this model is the opposite of that observed in model L1 except that the rich oil saturation zones in both models are located in the most permeable and porous regions of the reservoirs. The high oil saturation zone in either model is conical in shape but more like a screw with the wider top edge in the most permeable and porous layer and the narrow bottom end in the second to the smallest permeable and porous layer. These show that the mobilised oil that should have been produced earlier is forced to remain inside the reservoir and therefore, the chance of excessive thermal cracking leading to deposition of large concentration of coke is substantially increased especially in model L1 where the high oil saturation chambers are bigger and far away from the HP well. It is highlighted that this is quite unlike the results found for simulations conducted for an ideal homogeneous reservoir representative element (i.e. full efficient drainage of the mobilised partially upgraded oil). Furthermore, in model L2, the shape of mobile oil zone is nearly uniformly vertical as its location at the top and on the lateral edges are longitudinally the same. What is not clear, however, is the distance it has reached at the lower part of the longitudinal vertical mid-plane in the vicinity of the HP well. From the right lateral edge of the reservoirs of models L1 (Fig. 7a) and L2 (Fig. 7b), it appeared that almost the same volume of oil is left in the reservoir in either model. However, due to differences in residence times, and thus the fuel availabilities, and the horizontal sweeps, more oil is left in the reservoir of model L2.

With regard to comparing and contrasting between model L3

(Fig. 7c) and model L4 (Fig. 7d), it was found that two chambers with very high oil saturations were formed in the former, whilst, in the latter, no such high oil saturation zone exists. Furthermore, although higher areal sweep is achieved in the longitudinal vertical planes of the lateral edges of reservoir of model L3, the oil saturation on the large area of the lateral edges of model L4 has a value of at most 0.75, thereby implying that the areal sweep there is low. Moreover, more oil is drained around the mid-region of the reservoir of model L4, when compared to that in model L3. Similar to the preceding findings, the fluids tend to concentrate in the more permeable and porous region(s) of the reservoir, which is the case in model L3. In model L4, however, the most permeable and porous region is the vertical mid-plane within which the HP well is located, and, as a result, the fluids have a direct escape path, which is the reason why they did not concentrate there. These findings imply that drilling of the HP well on the vertical mid-plane of a reservoir, where the highest permeabilities and porosities are present, results in faster drainage of nearby fluids, as might be expected.

To find out how the oil saturation relates to the HP well at greater depth, cuts of the vertical mid-planes of all the models are shown in Fig. 8. From Fig. 8a and b, it is clear that there is higher areal sweep of oil in the vertical mid-plane of model L1 in comparison to that of model L2. This shows that more oil is left in the reservoir of model L2, which is in accordance with the earlier findings from the three-dimensional oil saturation distribution. Similarly, from Fig. 8c and d, it is found that more oil is left inside the reservoir in the former (i.e. model L3) compared to in the latter where larger areal sweep is achieved. To summarize, by the end of the 390 min of operation, a significant quantity of oil is left inside the reservoirs of models L2 and L3, when compared to those of models L1 and L4, respectively.

4. Conclusion

While gradations in petrophysical properties are likely to be very

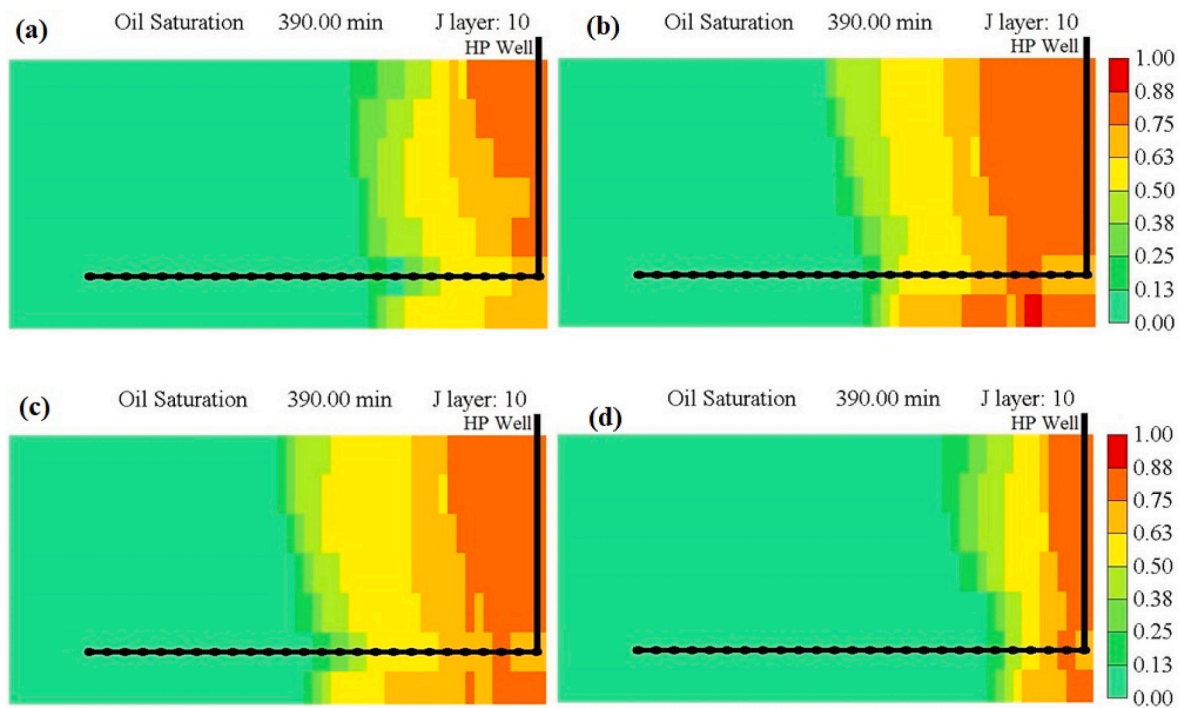


Fig. 8. Oil saturation distributions in the layered reservoirs at the end of 6 h of combustion and along the longitudinal vertical mid-planes of models (a) L1, (b) L2, (c) L3, and (d) L4 respectively.

common within sedimentary rocks, there has, previously, been little study of the effects of such gradations in reservoir petro-physical parameters on the performance of the THAI process. Consequently, this work reports the results of numerical simulation of four different kinds of reservoirs, each having progressive gradations in permeabilities and porosities. The major findings from this in depth study include:

- (i) In terms of the temperature distribution, regardless of the permeabilities and porosities gradations, the high temperature zone is always skewed towards the highest permeabilities and porosities zones. Furthermore, it is found that, in any model in which the shoes of the VI wells have no direct communication pathway with the highest permeabilities and porosities zones of the reservoirs, the high temperature zones occur in two chambers, otherwise there is but one high temperature zone.
- (ii) It is found that generally, the combustion front tends to be lopsided in favour of the most permeable and porous zones. In the case of model L1, the single combustion front has greatest advance horizontally at the top and axially in the middle of the reservoir, while in model L2, the combustion front propagated in two chambers before the chambers overlapped in the toe region of the HP well where it advanced fastest. Therefore, the combustion zone in model L1 is far more stable than in model L2.
- (iii) It is found that the combustion fronts in model L3 propagated in two chambers that overlapped each other around the toe region of the HP well and advanced greatest in the HP well and on either lateral edge of the reservoir. In model L4 however, the thinner edge of the wedge-shape combustion front has advanced fastest along the vertical mid-plane where the HP well is located. Thus, the combustion zone in model L3 is far more stable than that in model L4.
- (iv) It is found that in all the models except model L4, there exist rich oil saturation zones in the most permeable and porous regions located ahead of the mobile oil zone (MOZ) of each reservoir. These are formed due to restrictions in the pathways via which the mobilised oil can gravity-drain into the HP well. In model L4,

the HP well is already in the most permeable and porous zone, and, consequently, the fluids that favourably reach there are rapidly gravity-drained into the HP well. Furthermore, it is found that by the end of the 390 min of operation, significant quantity of oil is left inside the reservoirs of models L2 and L3, when compared to those of models L1 and L4, respectively.

Overall, the conventional THAI configuration, in which the foot of the HP well is located laterally in the middle and vertically near the base of the reservoir, works quite well in reservoirs with the top-down progressive decrease in permeabilities and porosities when compared to the same configuration in reservoirs with top-down progressive increase in permeabilities and porosities. For reservoirs with lateral gradations in permeabilities and porosities, the HP well should be located laterally in the least permeable and porous zones of the reservoir if stable combustion front propagation is the end goal at the expense of higher oil production rates. If the reverse is the end goal, then the HP well should be drilled in the most permeable and porous zones of the reservoir.

CRediT authorship contribution statement

Muhammad Rabiu Ado: Writing – review & editing, Writing – original draft, Visualization, Validation, Methodology, Investigation, Funding acquisition, Formal analysis, Data curation, Conceptualization. **Malcolm Greaves:** Writing – review & editing, Visualization, Validation, Supervision, Software. **Sean P. Rigby:** Writing – review & editing, Supervision, Software, Resources, Project administration, Funding acquisition.

Declaration of competing interest

The authors declare that they have no known competing financial interests or personal relationships that could have appeared to influence the work reported in this paper.

Data availability

Data will be made available on request.

Acknowledgment

The authors are grateful to the Computer Modelling Group (CMG) for supplying comprehensive reservoir simulator, the STARS.

References

- Ado, M.R., 2022a. Comparisons of predictive ability of Thai in situ combustion process models with pre-defined fuel against that having fuel deposited based on Arrhenius kinetics parameters. *J. Pet. Sci. Eng.* 208, 109716 <https://doi.org/10.1016/j.petrol.2021.109716>.
- Ado, M.R., 2022b. Electrically-enhanced Thai in situ combustion technology for upgrading and production of heavy oil. *J. Pet. Explor. Prod. Technol.* <https://doi.org/10.1007/s13202-022-01530-0>.
- Ado, M.R., 2021a. Use of two vertical injectors in place of a horizontal injector to improve the efficiency and stability of Thai in situ combustion process for producing heavy oils. *J. Pet. Explor. Prod. Technol.* <https://doi.org/10.1007/s13202-021-01345-5>.
- Ado, M.R., 2021b. Improving oil recovery rates in Thai in situ combustion process using pure oxygen. *Upstream Oil Gas Technol.*, 100032 <https://doi.org/10.1016/j.upstre.2021.100032>.
- Ado, M.R., 2021c. Understanding the mobilised oil drainage dynamics inside laboratory-scale and field-scale reservoirs for more accurate Thai process design and operation procedures. *J. Pet. Explor. Prod. Technol.* <https://doi.org/10.1007/s13202-021-01285-0>.
- Ado, M.R., 2021d. Improving heavy oil production rates in Thai process using wells configured in a staggered line drive (SLD) instead of in a direct line drive (DLD) configuration: detailed simulation investigations. *J. Pet. Explor. Prod. Technol.* <https://doi.org/10.1007/s13202-021-01269-0>.
- Ado, M.R., 2020a. Impacts of kinetics scheme used to simulate toe-to-heel air injection (Thai) in situ combustion method for heavy oil upgrading and production. *ACS Omega* 5. <https://doi.org/10.1021/acsomega.9b03661>.
- Ado, M.R., 2020b. A detailed approach to up-scaling of the Toe-to-Heel Air Injection (Thai) In-Situ Combustion enhanced heavy oil recovery process. *J. Pet. Sci. Eng.* 187 <https://doi.org/10.1016/j.petrol.2019.106740>.
- Ado, M.R., 2020c. Predictive capability of field scale kinetics for simulating toe-to-heel air injection heavy oil and bitumen upgrading and production technology. *J. Pet. Sci. Eng.* 187 <https://doi.org/10.1016/j.petrol.2019.106843>.
- Ado, M.R., 2020d. Simulation study on the effect of reservoir bottom water on the performance of the Thai in-situ combustion technology for heavy oil/tar sand upgrading and recovery. *SN Appl. Sci.* 2 <https://doi.org/10.1007/s42452-019-1833-1>.
- Ado, M.R., 2020e. Effect of reservoir pay thickness on the performance of the Thai heavy oil and bitumen upgrading and production process. *J. Pet. Explor. Prod. Technol.* 10 <https://doi.org/10.1007/s13202-020-00840-5>.
- Ado, M.R., Greaves, M., Rigby, S.P., 2022. Numerical simulation investigations of the applicability of Thai in situ combustion process in heavy oil reservoirs underlain by bottom water. *Pet. Res.* <https://doi.org/10.1016/j.ptres.2022.06.001>.
- Ado, M.R., Greaves, M., Rigby, S.P., 2019. Numerical simulation of the impact of geological heterogeneity on performance and safety of Thai heavy oil production process. *J. Pet. Sci. Eng.* 173 <https://doi.org/10.1016/j.petrol.2018.10.087>.
- Almeidaideb, R.A., Ashour, I., El-Fattah, K.A., 2003. Improved K-value correlation for UAE crude oil components at high pressures using PVT laboratory data. *Fuel* 82, 1057–1065.
- Anbari, H., Robinson, J.P., Greaves, M., Rigby, S.P., 2023. Field performance and numerical simulation study on the toe to heel air injection (Thai) process in a heavy oil reservoir with bottom water. *J. Pet. Sci. Eng.* 220, 111202.
- Boggs, S., 2006. *Principles of Sedimentology and Stratigraphy*, fourth ed. Pearson Prentice Hall, Upper Saddle River, NJ, pp. 94–97.
- Elahi, S.M., Scott, C.E., Chen, Z., Pereira-Almao, P., 2019. In-situ upgrading and enhanced recovery of heavy oil from carbonate reservoirs using nano-catalysts: upgrading reactions analysis. *Fuel* 252, 262–271. <https://doi.org/10.1016/j.fuel.2019.04.094>.
- Fietz, S.W., Maceachern, J.A., Gingras, M., Ranger, M., Dashtgard, S.E., 2024. Sedimentological and ichnological variations in fluvio-tidal translating point bars, McMurray Formation, Alberta, Canada. *Sedimentology* 71, 974–1022.
- Gates, I.D., 2010. Solvent-aided Steam-Assisted Gravity Drainage in thin oil sand reservoirs. *J. Pet. Sci. Eng.* 74, 138–146. <https://doi.org/10.1016/j.petrol.2010.09.003>.
- Gates, I.D., Larter, S.R., 2014. Energy efficiency and emissions intensity of SAGD. *Fuel* 115, 706–713. <https://doi.org/10.1016/j.fuel.2013.07.073>.
- Greaves, M., Dong, L., Rigby, S., 2012a. Validation of Toe-to-Heel air-injection bitumen recovery using 3D combustion-cell results. *SPE Reservoir Eval. Eng.* 15, 72–85.
- Greaves, M., Dong, L.L., Rigby, S., 2012b. Determination of limits to production in Thai. In: *SPE Heavy Oil Conf. Canada*. <https://doi.org/10.2118/157817-MS>.
- Greaves, M., Dong, L.L., Rigby, S.P., 2012c. Simulation study of the toe-to-heel air injection three-dimensional combustion cell experiment and effects in the mobile oil zone. *Energy Fuels* 26, 1656–1669.
- Greaves, M., El-Sakr, A., Xia, T.X., Ayasse, C., Turta, A., 1999. Thai - new air injection technology for heavy oil recovery and in situ upgrading. *Annu. Tech. Meet.* <https://doi.org/10.2118/99-15>.
- Greaves, M., Xia, T.X., Turta, A.T., 2008. Stability of Thai (TM) process - theoretical and experimental observations. *J. Can. Pet. Technol.* 47, 65–73.
- Guo, K., Li, H., Yu, Z., 2016. In-situ heavy and extra-heavy oil recovery: a review. *Fuel* 185, 886–902. <https://doi.org/10.1016/j.fuel.2016.08.047>.
- Hassanpour, R.M., 2009. A review of McMurray formation geology in Athabasca oil sands. *CCG Annual Report* 11. Paper 201.
- Le Ravalec, M., Morlot, C., Marmier, R., Foulon, D., 2009. Heterogeneity impact on SAGD process performance in mobile heavy oil reservoirs. *Oil Gas Sci. Technol. l'IFP* 64, 469–476.
- Liu, Z., Wang, H., Blackburn, G., Ma, F., He, Z., Wen, Z., Wang, Z., Yang, Z., Luan, T., Wu, Z., 2019. Heavy oils and oil sands: global distribution and resource assessment. *Acta Geol. Sin. - English* 199–212. <https://doi.org/10.1111/1755-6724.13778>. Ed. 93.
- Mojarab, M., Harding, T., Maini, B., 2011. Improving the SAGD performance by introducing a new well configuration. *J. Can. Pet. Technol.* 50, 9–18.
- Oskouei, S.J.P., Moore, R.G., Maini, B., Mehta, S., 2011. Feasibility of in-situ combustion in the SAGD chamber. *J. Can. Pet. Technol.* 50, 31–44.
- Rabiu Ado, M., 2017a. Numerical simulation of heavy oil and bitumen recovery and upgrading techniques [WWW Document]. URL. <http://eprints.nottingham.ac.uk/41502/>. accessed 5.20.19.
- Rabiu Ado, M., Greaves, M., Rigby, S.P., 2018. Effect of pre-ignition heating cycle method, air injection flux, and reservoir viscosity on the Thai heavy oil recovery process. *J. Pet. Sci. Eng.* 166 <https://doi.org/10.1016/j.petrol.2018.03.033>.
- Rabiu Ado, M., Greaves, M., Rigby, S.P., 2017b. Dynamic simulation of the toe-to-heel air injection heavy oil recovery process. *Energy Fuel*. 31 <https://doi.org/10.1021/acs.energyfuels.6b02559>.
- Shah, A., Fishwick, R., Wood, J., Leeke, G., Rigby, S., Greaves, M., 2010. A review of novel techniques for heavy oil and bitumen extraction and upgrading. *Energy Environ. Sci.* 3, 700–714. <https://doi.org/10.1039/b918960b>.
- Shi, L., Xi, C., Liu, P., Li, X., Yuan, Z., 2017. Infill wells assisted in-situ combustion following SAGD process in extra-heavy oil reservoirs. *J. Pet. Sci. Eng.* 157, 958–970. <https://doi.org/10.1016/j.petrol.2017.08.015>.
- Thomas, R.G., Smith, D.G., Wood, J.M., Visser, J., Calverley-Range, E.A., Koster, E.H., 1987. Inclined heterolithic stratification- terminology, description, interpretation and significance. *Sediment. Geol.* 53, 123–179.
- Turta, A., Singhal, A., 2004. Overview of short-distance oil displacement processes. *J. Can. Pet. Technol.* 43.
- Wang, Y., Ren, S., Zhang, L., 2019. Mechanistic simulation study of air injection assisted cyclic steam stimulation through horizontal wells for ultra heavy oil reservoirs. *J. Pet. Sci. Eng.* 172, 209–216. <https://doi.org/10.1016/j.petrol.2018.09.060>.
- Wei, W., Rezazadeh, A., Wang, J., Gates, I.D., 2020a. An analysis of toe-to-heel air injection for heavy oil production using machine learning. *J. Pet. Sci. Eng.* 108109 <https://doi.org/10.1016/j.petrol.2020.108109>.
- Wei, W., Wang, J., Afshordi, S., Gates, I.D., 2020b. Detailed analysis of Toe-to-Heel Air Injection for heavy oil production. *J. Pet. Sci. Eng.* 186, 106704 <https://doi.org/10.1016/j.petrol.2019.106704>.
- Xia, T., Greaves, B., Werfilli, M., Rathbone, R., 2002. Thai process-effect of oil layer thickness on heavy oil recovery. In: *Canadian International Petroleum Conference*.
- Xia, T., Greaves, M., 2006. In situ upgrading of Athabasca tar sand bitumen using Thai. *Chem. Eng. Res. Des. - CHEM ENG RES DES* 84, 856–864. <https://doi.org/10.1205/cherd.04192>.
- Xia, T., Greaves, M., Turta, A., 2005. Main mechanism for stability of Thai-Toe-to-Heel air injection. *J. Can. Pet. Technol.* 44.
- Xia, T.X., Greaves, M., 2002. Upgrading Athabasca tar sand using toe-to-heel air injection. *J. Can. Pet. Technol.* 41, 7. <https://doi.org/10.2118/02-08-02>.
- Zhao, D.W., Wang, J., Gates, I.D., 2014. Thermal recovery strategies for thin heavy oil reservoirs. *Fuel* 117, 431–441. <https://doi.org/10.1016/j.fuel.2013.09.023>.
- Zhao, D.W., Wang, J., Gates, I.D., 2013. Optimized solvent-aided steam-flooding strategy for recovery of thin heavy oil reservoirs. *Fuel* 112, 50–59. <https://doi.org/10.1016/j.fuel.2013.05.025>.
- Zhao, R., Li, B., Yang, X., Yang, J., Yu, S., Jin, J., Zhang, J., 2018a. Analysis of a feasible Thai pattern by the derivation of scaling criteria and combustion experiments. *J. Pet. Sci. Eng.* 168, 380–389. <https://doi.org/10.1016/j.petrol.2018.05.022>.
- Zhao, R., Yang, J., Zhao, C., Heng, M., Wang, J., 2021. Investigation on coke zone evolution behavior during a Thai process. *J. Pet. Sci. Eng.* 196, 107667 <https://doi.org/10.1016/j.petrol.2020.107667>.
- Zhao, R., Yu, S., Yang, J., Heng, M., Zhang, C., Wu, Y., Zhang, J., Yue, X., 2018b. Optimization of well spacing to achieve a stable combustion during the Thai process. *Energy* 151, 467–477. <https://doi.org/10.1016/j.energy.2018.03.044>.